



Deposited via The University of Leeds.

White Rose Research Online URL for this paper:

<https://eprints.whiterose.ac.uk/id/eprint/155137/>

Version: Accepted Version

Article:

Wang, H, Lin, G, Bai, L et al. (2020) Comparative study of two loop heat pipes using R134a as the working fluid. Applied Thermal Engineering, 164. 114459. ISSN: 1359-4311

<https://doi.org/10.1016/j.applthermaleng.2019.114459>

© 2019 Elsevier Ltd. All rights reserved. This manuscript version is made available under the CC-BY-NC-ND 4.0 license <http://creativecommons.org/licenses/by-nc-nd/4.0/>.

Reuse

This article is distributed under the terms of the Creative Commons Attribution-NonCommercial-NoDerivs (CC BY-NC-ND) licence. This licence only allows you to download this work and share it with others as long as you credit the authors, but you can't change the article in any way or use it commercially. More information and the full terms of the licence here: <https://creativecommons.org/licenses/>

Takedown

If you consider content in White Rose Research Online to be in breach of UK law, please notify us by emailing eprints@whiterose.ac.uk including the URL of the record and the reason for the withdrawal request.

Comparative study of two loop heat pipes using R134a as the working fluid

Huanfa Wang¹, Guiping Lin¹, Lizhan Bai^{1,*}, Yongbo Tao¹, Dongsheng Wen^{1,2}

¹ Laboratory of Fundamental Science on Ergonomics and Environmental Control, School of Aeronautic Science and Engineering, Beihang University, Beijing 100191, PR China

² School of Chemical and Process Engineering, University of Leeds, Leeds, LS2 9JT, UK

Abstract: In order to promote future commercial applications of loop heat pipe (LHP) especially in the civil fields, environmentally friendly R134a is considered a good candidate working fluid to replace the commonly used anhydrous ammonia. In this work, two sets of LHPs with R134a as the working fluid were designed and fabricated, one with a nickel wick, and the other with a stainless steel wick. Their thermal performance, mainly including the startup, the power increment test, the thermal resistance and the heat transport capability, were experimentally studied, evaluated and compared. Based on the experimental results, it is found that both of the R134a LHPs present excellent startup performance, achieve a maximum heat transfer capacity greater than 100 W, and exhibit good response characteristics to stepwise change of heat load. The R134a LHP with a nickel wick shows good anti-gravity capability; however, the one with a stainless steel wick is quite sensitive to the adverse elevation. The physical mechanisms responsible for the experimental results mentioned above have been analyzed and discussed. This work contributes to a better understanding on the operating performance and characteristics of the R134a LHPs, providing good design guidance and reference for its future applications.

Keywords: loop heat pipe; R134a; startup; heat transfer; thermal resistance

* Corresponding author. Tel.: +86 10 8233 8600; Fax: +86 10 8233 8600

E-mail address: bailizhan@buaa.edu.cn (L. Bai)

1 Introduction

With the fast development of modern electronic and telecommunication industry, electronics cooling is increasingly becoming an issue to be addressed. For instance, modern computers have become one of the most important working tools nowadays, and its processing speed is keeping increasing, leading to an obvious increase in both the power consumed and the heat to be dissipated. In addition, as computers are developing towards miniaturization and compactness, the traditional aluminum fin heat sink cannot meet the cooling requirements anymore. As the core component, the CPU would suffer from serious performance degradation and even destruction without the employment of an efficient and effective cooling method [1]. That is because electronics cooling is of great importance in maintaining the normal operation of electronic devices and modules, especially when the power density becomes relatively large. With the increase of the operating temperature, both the operating performance and reliability of electronic devices decrease; and once the device temperature exceeds its maximum allowable value, an operation failure will occur. In particular, at very high temperatures even a burn-out may happen, causing serious unexpected accidents. As the heat flux generated from the electronic devices keeps an ever-growing trend, it continuously imposes new challenge to the cooling technology.

With the development of electronics cooling technology, heat pipe has already been widely applied in a variety of cooling systems [2-8]. However, traditional heat pipe generally suffer from the heat transfer limit under the condition without the assistance of gravity. As a highly efficient and reliable two-phase heat transfer device, loop heat pipe (LHP) holds significant application potential in the modern electronics cooling. It utilizes the phase change of evaporation and condensation of a working fluid to transfer heat, and relies on the capillary forces developed in the evaporator wick to circulate the working fluid inside a closed loop where no external power is required [9]. Compared with traditional heat pipe, significant

structural improvement has been made for LHP, mainly including the local installment of porous wick, the employment of inverted evaporator as well as the separation of liquid/vapor transport lines. These structural improvement effectively overcomes the inherent drawback of conventional heat pipe such as small heat transfer capacity, weak antigravity capability and unfavorable flexibility in installment, enabling LHP to be a more universal and advanced heat transfer device [10-15]. Its long distance heat transport capability and flexibility in packaging as well as strong antigravity operation show obvious advantages over traditional heat pipes [16-27]. As a result, it has been well accepted in the future electronics cooling, to provide a low noise and power-saving solution.

Besides the high performance wick located in the evaporator, the thermal performance of a LHP is strongly dependent on the working fluid charged inside the loop, which determines its operating temperature range, heat transport capability and heat transfer performance. For a LHP operating at the ambient temperature range, i.e., 0-60 °C, anhydrous ammonia is generally considered to be the best choice compared with other working fluids, only considering the heat transfer performance and heat transport capacity. That is because ammonia has very good comprehensive thermo-physical properties, i.e., large surface tension and evaporative latent heat, large vapor density, small liquid viscosity and relatively high thermal conductivity of liquid. What's more, it has very high saturation pressure difference corresponding to unit temperature difference $(dP/dT)_{sat}$, enabling the ammonia-charged LHP to produce rather small temperature difference between the evaporator and the condenser during the steady-state operation, and quite favorable heat transfer performance and heat transport capability can be achieved accordingly.

Although ammonia-charged LHP exhibits excellent heat transfer performance and high heat transport capability, it is generally not allowed to be commercially used, especially in an environment where people are present. That is because anhydrous ammonia is a toxic substance, which will destroy the environment and lead

to serious health hazard to the people around once a working fluid leakage occurs, especially in a closed finite space. In fact, the saturation pressure of ammonia at 60 °C is as high as 25.8 atm, and generally the risk of fluid leakage cannot be absolutely avoided. Due to the safety and health issues caused by the use of ammonia, there is an orientation to replace this substance by other working fluids of lower risk and easier to handle. To expand the application area of LHP especially in a manned environment, it is essential to explore alternative working fluids with less risk or no risk. Currently, there are two kinds of candidate working fluids that may be suitable for LHP. For one kind of working fluid, it is still toxic to some extent; however, its saturation pressure at the ambient temperature is quite close to the atmospheric pressure, even below the atmospheric pressure, so the leakage risk can be reduced significantly. Typical working fluids of this kind include acetone, methanol, ethanol, water, etc. For the other kind, although its saturation pressure at the ambient temperature may be still very high, and the leakage risk still exists, it is non-toxic and environmentally friendly. Typical working fluids of this kind are mainly Freons, such as R134a and R22.

Considering the safety and health issues for an ammonia-charged LHP, when the heat load to be dissipated is not very large, i.e., at the level of 100-200W, R134a becomes an interesting option for the working fluid of a LHP. That is because R134a is a common refrigerant, which has been widely used in the air conditioning and refrigeration systems. Its critical temperature and freezing temperature are 101.1 and -96.6 °C, respectively. It indicates that the normal operation of a two-phase heat transfer system at a relatively wide temperature range can be ensured with no freezing hazard. Different from many other freons, R134a is quite environmentally friendly because it contains no chlorine atoms, producing no destructive effect on ozone layer. R134a also demonstrates very good safety performance i.e., non-flammable, non-explosive, non-toxic and non-irritating, which is quite applicable in the civilian field. In addition, R134a is also compatible with the engineering metal materials commonly used for LHP

fabrication, such as the stainless steel, nickel, copper and aluminum.

To date, relevant studies on LHPs with R134a as the working fluid, both experimental and theoretical, are quite few, as briefly reviewed below. Kobayashi et al. [28] fabricated a flexible LHP using R134a as the working fluid. For the LHP, the evaporator and condenser were connected by long flexible tubes with a diameter of 3 mm, and the total piping length was approximately 7500 mm. Porous Teflon with an effective pore diameter of 1.2 μm was selected as the primary wick material to overcome high gravitational heads. Elevation of the evaporator above the condenser (ΔH) was changed in three conditions ($\Delta H = +1, 0$ and -1 m) considering the terrestrial application, and the influence of gravity on the LHP performance was investigated. Experimental results showed that the LHP provided high thermal transport capacity over long distances through small cross-sectional flexible tubes compared with conventional heat pipes. An analysis method to predict the maximum heat transfer rate of the LHP was also proposed by the authors. Adoni et al. [29-30] experimentally investigated a LHP using R134a as the working fluid. The evaporator wick was made of ultra-high molecular weight (UHMW) polyethylene. It was found that the liquid inventory in the compensation chamber can significantly influence the operating characteristics of the LHP. The large liquid inventory in the compensation chamber under terrestrial conditions could result in the loss of thermal coupling between the compensation chamber and the evaporator core. This caused the operating temperature to increase monotonically. They also experimentally determined the evaporation heat transfer coefficients for the LHP with acetone, R134a and ammonia as the working fluids respectively, and analyzed the influences of working fluid, hydrodynamic blocks in the core, evaporator configuration and adverse elevation (evaporator above condenser) on the heat transfer coefficient. Experimental results indicated that ammonia exhibited the highest heat transfer coefficient among the working fluids studied. Nishikawara et al. [31] fabricated a miniature LHP with a polytetrafluoroethylene (PTFE) wick, and its evaporator

thermal performance was investigated with parametric experiments. Ethanol, acetone and R134a were charged in the LHP to evaluate the effect of the properties of the working fluids. According to the experimental results, the maximum heat load of the LHP was observed for acetone, followed in order by ethanol and R134a. This order agrees with the results of the values of the figure of merit of these working fluids. While the pressure difference of transport lines with R134a was the smallest of all, due to its large vapor density at a high working pressure.

R134a-charged LHP exhibits great potential in commercial applications. In order to push forward its future practical applications, a comprehensive and in-depth study is really needed to characterize its operation and guide its design. There are still many questions for R134a-charged LHPs to be addressed. In the previous studies, the R134a-charged LHP typically used a primary wick made of UHMW polyethylene or polytetrafluoroethylene due to their much reduced thermal conductivity. Is it feasible to employ a primary wick made of nickel or stainless steel powders is still unknown. The minimum heat load required to start up a R134a-charged LHP is seldom reported, which is indeed a very important topic and needs to be well studied before its practical applications, because it will influence whether an auxiliary measure should be employed to assist the startup at small heat loads. In addition, how and to what extent the adverse elevation may affect the heat transfer performance especially the heat transport capability of a R134a-charged LHP with a nickel or stainless steel wick are still not well answered. The underlying influencing mechanisms need to be well explored and revealed. To better understand and characterize its operating characteristics, and also to provide a guidance for the design of R134a-charged LHPs, the issues mentioned above should be appropriately addressed, which forms the main objective of this work.

2 Experimental setup

Two sets of LHPs using R134a as the working fluid were designed and fabricated in this work, which

were called LHP-1 and LHP-2, respectively. For LHP-1 and LHP-2, the only difference was the evaporator size and material. LHP-1 employed an evaporator wick made of nickel powders, while for LHP-2 the evaporator wick was made of stainless steel powders. Table 1 presents the basic parameters of the two LHPs, where OD represents the outer diameter, and ID represents the inner diameter, respectively.

Fig. 1 (a) shows the basic structure of a LHP with a cylindrical evaporator, which is composed of an evaporator, a compensation chamber (CC), a condenser and liquid and vapor transport lines, and Fig. 1 (b) shows the internal structure of the evaporator and CC. Figs. 2 and 3 show the 3-D structure of the evaporators of the LHP-1 and LHP-2, respectively. Heat load was applied to the evaporator in different ways for LHP-1 and LHP-2. For LHP-1, a thin film electric resistance heater was attached directly to the evaporator casing; while for LHP-2, a cartridge heater was employed, which was connected to the evaporator casing through an aluminum saddle. In order to reduce the contact thermal resistance, the contact surfaces were covered by thermal grease before assembling. Both heaters (film heater and cartridge heater) were connected to a regulated DC power supply, of which the relative uncertainty was within 6.0%. The two LHPs adopted one same condenser as displayed in Fig. 4. The condenser line was embedded into a copper cold plate, which was cooled by the circulating water at a constant temperature. The water temperature was easily to be adjusted, which was controlled by a thermostatic trough with an uncertainty of about ± 0.5 °C.

Fifteen type-T thermocouples with an uncertainty of about ± 0.5 °C were employed to monitor the temperature profile along the loop, as illustrated in Figs. (2-4). TC4 and TC11 were located at the middle of the vapor line and liquid line respectively, which were not shown in the figures. The ambient temperature was measured by TC15. Temperature data from the thermocouples was recorded, displayed and stored every five seconds by a data acquisition system (Agilent 34970A) linked to a PC. In order to simulate the

real situation of LHP application as much as possible, no thermal insulation was adopted for the casing of the LHP in the experiment. Only the thermocouple junction was covered by a layer of thermal insulation material to reduce the heat transfer to the environmental surroundings, so that the measured wall temperatures should be very close to the temperatures of the working fluid inside, as the wall thickness was no more than 1.0 mm for all the LHP components.

3 Experimental results and discussions

3.1 Startup

To push forward the practical applications of LHPs, the startup is always the first and most important issue to be addressed. As a passive heat transfer device, generally a LHP can realize self-startup without any preconditioning. However, self-startup does not mean instant startup, and the startup may take a long time accompanied by very large evaporator temperature rise, especially when the startup heat load is relatively small [32-33]. As a two-phase heat transfer device, the startup of a LHP is a very complex dynamic process, ranging from the application of a heat load to the evaporator to the normal circulation of working fluid in the loop. During this process, a variety of heat transfer phenomena such as evaporation, boiling, condensation and convection may be involved, accompanied by complicated liquid/vapor movement and phase redistribution. According to previous studies, the startup of a LHP may be affected by multiple factors such as the initial liquid/vapor distribution in the evaporator, the startup heat load, element geometry, adverse elevation and the non-condensable gas. Based on the initial liquid/vapor distribution in the evaporator, four possible startup situations have been identified, as listed in Table 2. Many experiments have shown that LHPs are the easiest to start up in situation 2, but the most difficult in situation 3. In this work, the startup experiments were all carried out under a horizontal orientation, i.e., the evaporator was kept horizontal with the condenser.

3.1.1 Startup characteristics of LHP-1

Fig. 5 shows the temperature change of some characteristic points along the loop during the startup process of LHP-1. In Fig. 5, the startup heat load was 5 W, and the heat sink temperature was set as 20 °C. As shown in Fig. 5, an obvious “temperature overshoot” occurred during the startup process, i.e., the evaporator temperature first rose to a peak value about 29.2 °C, then it began to drop gradually until reaching a steady state operating temperature of about 26.5 °C.

After the heat load was applied to the evaporator, TC13 on the top of the CC rose almost simultaneously with TC1 on the electric heater, while TC3 at the evaporator outlet rose very slightly. Such a phenomenon should correspond to the situation when the vapor grooves are flooded by liquid and a liquid/vapor interface exists in the CC, i.e., the startup situation 3 in Table 2, which is considered to be the most difficult case to realize the startup of LHPs. In this scenario, as a result of the absence of liquid/vapor interface in the vapor grooves, an instant evaporation in the vapor grooves with the application of the heat load is generally impossible; instead a certain liquid superheat will be required to initiate the nucleate boiling first. At the same time, the quick increase of the CC temperature leads to an increase of the saturation pressure in the loop, which is detrimental to the formation of required superheat in the vapor grooves, and a relatively large temperature rise is necessary for the evaporator in the startup. Once the nucleate boiling occurred in the vapor grooves, the evaporator temperature would drop rapidly due to the heat absorption by the liquid evaporation. With the circulation of the working fluid in the loop, a steady-state operating temperature would be reached eventually when each component of the LHP achieved the energy and pressure balance.

Fig. 6 shows another startup test of LHP-1 with the same heat load of 5 W. Much different from the case in Fig. 5, a very smooth startup process with no temperature overshoot appears in Fig. 6. As shown in Fig. 6, when heat load was applied to the evaporator, TC3 at the evaporator outlet rose quickly together with the

evaporator temperature TC2, indicating that vapor should initially exist in the vapor grooves, and no obvious superheat is required for the vapor generation. At the same time, TC13 on the top of the CC also rose fast with the evaporator temperature, which shows that liquid/vapor interface should exist in the evaporator core, resulting in relatively large heat leak from the evaporator to the CC. Therefore this startup corresponds to the situation 4 in Table 2, and very favorable startup performance can be expected.

Figs. 7 and 8 show the temperature change of some characteristic points along the loop during the startup process of LHP-1 at the startup heat loads of 20 and 40 W respectively. In Figs. 7 and 8, the variation characteristics of the temperature curves are quite similar to those in Fig. 6, indicating that both startups should correspond to the situation 4 in Table 2, and quite satisfactory startup performance has been achieved. In fact, the startup tests for LHP-1 were conducted for more than twenty times, and in most cases it started up in situation 4 with excellent startup performance where no any startup failure occurred.

In Figs. 5 and 7, the evaporator outlet temperature (TC3) is obviously higher than the CC inlet temperature (TC12) after the circulation of the working fluid in the loop during the startup; while in Figs. 6 and 8, the CC inlet temperature (TC12) is very close to or slightly higher than the evaporator outlet temperature (TC3). According to the fundamental operation principle of the LHP, the CC inlet temperature (TC12) should always be lower than the evaporator outlet temperature (TC3), and the experimental results in Figs. 6 and 8 seems unreasonable. However, it should be of note that the difference between the evaporator outlet temperature and the CC inlet temperature in Figs. 6 and 8 is always within 0.23 °C, and the authors think it is reasonable considering the uncertainty of the temperature measurement (± 0.5 °C) in the experiment.

3.1.2 Startup characteristics of LHP-2

Fig. 9 shows the temperature change of some characteristic points along the loop during the startup

process of LHP-2. In Fig. 9, the startup heat load was 2 W, and the heat sink temperature was set as 20 °C. As shown in Fig. 9, an obvious “temperature overshoot” occurred during the startup process, i.e., the evaporator temperature first rose to a peak value about 24.6 °C, then it dropped sharply to about 22.8 °C followed by a gradual increase until reaching a steady state operating temperature of about 24.0 °C.

After the heat load was applied to the evaporator, TC13 on the top of the CC remained almost unchanged, indicating that the evaporator core should be flooded by liquid and the heat leak from the evaporator to the CC is very small. While TC2 on the evaporator and TC3 at the evaporator outlet rose quickly, indicating that vapor should exist in some vapor grooves, and evaporation occurs there instantly with the application of the heat load. The sudden drop of the evaporator temperature TC2 after reaching the peak value suggests that some vapor grooves should be flooded by liquid, and the occurrence of nucleate boiling there leads to intensive absorption of the sensible heat of the evaporator casing. A large amount of vapor bubbles were generated at the outer side of the wick, causing a sharp increase of the local pressure. A majority of vapor flowed out of the evaporator and entered the condenser, as evidenced by a sharp increase of the temperature at the condenser inlet TC5. Some vapor penetrated the wick and entered the CC, leading to a sudden increase of the CC temperature TC13. Based on the analysis above, this startup should correspond to a mixture of situation 1 and 2 in Table 2. With the circulation of the working fluid along the loop, the LHP-2 finally reached a steady state when each component achieved the energy and pressure balance.

Figs.10-12 show the temperature change of some characteristic points along the loop during the startup process of LHP-2 at the startup heat loads of 20, 40 and 80 W respectively. In Figs. 10-12, the variation characteristics of the temperature curves are quite similar to those in Fig. 6, indicating that both startups should correspond to the situation 4 in Table 2, and quite satisfactory startup performance has been achieved with no occurrence of temperature overshoot. In fact, the startup tests for LHP-2 were also

conducted for more than twenty times, and in most cases it started up in situation 4 with excellent startup performance where no any startup failure was observed.

3.1.3 Comparison study on the startup

The startup performance is a key indicator in evaluating the thermal performance of a LHP, greatly affecting its future practical applications. In this work, both LHP-1 and LHP-2 exhibit very excellent startup performance. They can both start up successfully with a very small heat load, and no large temperature overshoot appears. To be specific, LHP-1 can start up with a heat load of 5 W corresponding to a heat flux of 1666 W/m^2 , and LHP-2 can start up with a heat load of 2 W corresponding to a heat flux of 700 W/m^2 . For both LHP-1 and LHP-2, the maximum temperature overshoot is less than $2.0 \text{ }^\circ\text{C}$ even in the most difficult startup scenario. According to the experimental results, in most cases both LHP-1 and LHP-2 started up in situation 4 with excellent startup performance where no any startup failure was observed. However, LHP-1 was observed to start up in situation 3 occasionally, and LHP-2 was observed to start up in a mixture of situations of 1 and 2 once in the experiments.

Generally, for an ammonia-charged LHP, when the heat load is very small, i.e., $< 10 \text{ W}$, a very large temperature overshoot may appear, and even a startup failure may occur. As shown in Fig. 13, for an ammonia-charged LHP, when the heat load was 5 W corresponding to a heat flux of 1666 W/m^2 , a very large temperature overshoot greater than $30 \text{ }^\circ\text{C}$ was observed, and the maximum evaporator temperature during the startup process exceeded $60 \text{ }^\circ\text{C}$ [34]. That is because at a small startup heat load, on one hand, the required temperature/pressure difference between the evaporator and the CC is difficult to establish, to drive the normal circulation of the working fluid along the loop; on the other hand, as the mass flowrate in the loop is generally very small under this condition, the cooling effect of the return subcooled liquid on the CC becomes very weak. These two combined effects should be responsible for the very large temperature

overshoot.

Different from ammonia-charged LHPs, both LHP-1 and LHP-2 studied in this work can start up successfully with a quite small heat load, and no large temperature overshoot appears, which is a unique advantage compared with ammonia-charged LHPs. Therefore, for LHP with R134a as the working fluid, no auxiliary measures are needed to assist its startup, making it a totally passive two-phase heat transfer device.

In the authors' opinion, good startup performance at small heat loads is closely associated with two thermophysical properties of the working fluid: high $(dP/dT)_{\text{sat}}$ and relatively small evaporative latent heat, by considering the energy balance of the CC. A large value of $(dP/dT)_{\text{sat}}$ means that the LHP can generate sufficient driving force with a very small temperature difference between the evaporator and the CC, and under which condition, the heat leak from the evaporator to the CC becomes very small. As illustrated in Table 3, the $(dP/dT)_{\text{sat}}$ values of R134a and ammonia are about 17.7 and 27.4 kPa/°C at 20 °C, which are both very high and beneficial to improve the startup performance. However, the evaporative latent heat of ammonia (1160.0 kJ/kg) is much larger than that of R134a (182.4 kJ/kg), and large evaporative latent heat leads to small mass flowrate of the working fluid in the loop, which is crucial in affecting the cooling effect of the return subcooled liquid on the CC. The much smaller evaporative latent heat of R134a should be responsible for the much better startup performance compared with an ammonia-charged LHP. However, much smaller evaporative latent heat may also lead to much reduced heat transport capability of the LHP, as reported later.

3.2 Power increment test

The power increment test was conducted under a horizontal orientation. The LHP was started up at a heat load of 20 W, and the heat load was increased stepwise with an interval of 20 W. For safety consideration, the vapor temperature at the evaporator outlet measured by TC3 was monitored carefully. In the experiment,

the maximum vapor temperature should be kept below 70 °C, at which the internal pressure in the loop was about 2.1 MPa. When the internal pressure was larger than 2.7 MPa, irreversible deformation and damage might occur for the LHP casing.

3.2.1 Transient characteristics

Figs. 14 and 15 display the transient thermal responses of LHP-1 and LHP-2 in the power increment tests respectively. As a whole, the transient thermal responses were quick and smooth for both LHP-1 and LHP-2 when the heat load was increased. Only a slight temperature overshoot with a value of about 1.5 °C was observed on the evaporator of LHP-2 when the heat load was changed from 20 to 40 W, as shown in Fig. 15. By analyzing the temperature evolutions of the condenser and liquid line, the temperature overshoot might be associated with the significant temperature drop at the CC inlet TC12.

In addition, significant differences in the condenser temperature variation characteristics of the two LHPs could also be observed. When the heat load was increased from 20 to 60 W, the condenser utilization of LHP-1 increased continuously, and temperature fluctuation could be observed on the condenser when the heat load was lower than 60 W. On the contrary, the condenser utilization of LHP-2 was always kept the maximum, and no temperature fluctuation was observed in the whole heat load range.

3.2.2 Steady-state characteristic and thermal resistance analysis

The steady-state operating characteristics of LHP-1 and LHP-2 were presented in Figs. 16 and 17 respectively. The heat source temperature was represented by TC1 on the film heater surface or aluminum saddle, and the saturation temperature of the CC was determined by TC13 on the top of the CC because the bottom of the CC was usually filled with subcooled liquid. Considering the temperature distribution along the condenser line, the temperature of the condenser was approximately determined by the average temperature of TCs (5-10) in this study. The heat transfer limits, i.e., the maximum heat load the LHP

evaporator can sustain, were 100 and 120 W for LHP-1 and LHP-2 respectively, with the vapor temperature (TC3) not exceeding 70 °C. The maximum heat flux for LHP-1 and LHP-2 were about 33200 and 42000 W/m² respectively. The relatively small heat transfer limit resulted from the low figure of merit value, which was commonly used for working fluid evaluation and selection for LHPs. Actually, the figure of merit of R134a was about an order of magnitude lower than that of ammonia in the temperature range of 0-60 °C.

As shown in Fig. 16, the operating temperature of LHP-1 increased approximately linearly with the increase of the heat load. A minimum vapor temperature of 25.2 °C and a maximum vapor temperature of 49.3 °C was obtained at a heat load of 20 and 100 W respectively. In addition, the temperature difference among the evaporator, condenser and CC was quite small, which was no more than 8.0 °C even when the heat load was 100 W. This indicated that the evaporator did not overheat greatly and a relatively high heat transfer efficiency could be achieved.

Different from the temperature characteristics of LHP-1, the steady state operating temperature of LHP-2 exhibited a typical “U-shaped” curve with the increase of heat load, as shown in Fig. 17. The minimum steady state vapor temperature obtained in this experiment was at about 33.8 °C, corresponding to a heat load of 40 W. Actually, the vapor temperature remained lower than 50 °C up to heat loads close to 80 W. The temperatures of the vapor line and CC were almost the same until the heat load was 60 W, and a large temperature difference between them was observed when the heat load was larger than 60 W. This indicated that there should be a large superheat for the vapor when the heat load was relatively large.

Thermal resistance is one of the most significant parameters that characterizes the efficiency of a heat transfer system, and a low thermal resistance of the heat transfer device reflects the high heat transfer performance. Thermal resistance analysis shows that the thermal resistance of the LHP-based heat transfer

system studied here consists of three parts: the thermal resistance from the heat source to the evaporator casing R_{hs-ev} , the thermal resistance of the LHP itself R_{LHP} and the thermal resistance from the condenser wall to the heat sink $R_{cond-sink}$. The total thermal resistance of the “heat source-LHP-heat sink” heat transfer system $R_{hs-LHP-sink}$ is the sum of the three thermal resistances mentioned above, which can be written as:

$$R_{hs-LHP-sink} = R_{hs-ev} + R_{LHP} + R_{cond-sink} \quad (1)$$

In the present study, the thermal resistance of the overall “heat source-LHP-heat sink” heat transfer system can be calculated by the formula:

$$R_{hs-LHP-sink} = \frac{T_{hs} - T_{sink}}{Q} \quad (2)$$

where T_{hs} was the temperature of the heat source, which can be represented by TC1. Q is the heat load applied to the evaporator, and T_{sink} is the heat sink temperature, which is set as 20 °C in this study.

The thermal resistance from the heat source to the evaporator can be calculated by the following equation:

$$R_{hs-ev} = \frac{T_{hs} - T_{ev}}{Q} \quad (3)$$

where T_{ev} is the temperature of evaporator casing, which can be represented by TC2.

The thermal resistance of the LHP was usually determined by the temperature of evaporator casing and the average temperature of the condenser, which can be calculated as follows:

$$R_{LHP} = \frac{T_{ev} - T_{cond}}{Q} \quad (4)$$

The thermal resistance from the condenser wall to the heat sink $R_{cond-sink}$ is the difference between the condenser temperature and the heat sink temperature divided by the supplied heat load, which can be written as

$$R_{\text{cond-sink}} = \frac{T_{\text{cond}} - T_{\text{sink}}}{Q} \quad (5)$$

With each thermal resistance clearly defined, the thermal resistance analysis of the “heat source-LHP-heat sink” heat transfer system with R134a as the working fluid can be carried out, and the experimental results are displayed in Fig. 18. The thermal resistance from the heat source to the evaporator casing is determined by the characteristics of the thermal contact between the heat source and the evaporator, which is affected by a variety of factors. In this study, although the heating methods of the two LHPs were quite different, the thermal resistance from the heat source to the evaporator casing was roughly at the same level, and the maximum value was no more than 0.5 °C/W.

In general, the thermal resistance from the condenser wall to the heat sink reflects the cooling efficiency of the condenser. In this study, the $R_{\text{cond-sink}}$ of LHP-1 almost remained at the same value, which was about 0.21~0.23 °C/W. Different from LHP-1, the $R_{\text{cond-sink}}$ of LHP-2 decreased slightly with the increase of the heat load. More precisely, the maximum and minimum value of the $R_{\text{cond-sink}}$ of LHP-2 was 0.24 °C/W and 0.17 °C/W respectively. As the structure and size of the two condensers were all the same, the difference could be mainly attributed to the variation in the utilization efficiency of the condenser, which reflected the part of the two-phase zone in the condenser. As mentioned earlier in section 3.2.1, in the experiments LHP-1 achieved a maximum utilization efficiency of the condenser at 20W, while the utilization efficiency of the condenser for LHP-2 increased with the increase of the heat load continuously.

The thermal resistance range of LHP-1 was 0.033~0.050 °C/W when the heat load was increased from 20 to 100 W. Compared with the other two thermal resistances $R_{\text{hs-ev}}$ and $R_{\text{cond-sink}}$, the thermal resistance of the LHP was about an order of magnitude lower, which reflected the advantage of LHP in the heat transfer performance. Such a small thermal resistance is closely related to the high $(dP/dT)_{\text{sat}}$ value of R134a working fluid. In general, if the LHP is designed appropriately, the higher the value of $(dP/dT)_{\text{sat}}$, the

smaller the thermal resistance of the LHP.

However, the thermal resistance of LHP-2 was relatively large, which became a dominant component of the total thermal resistance, quite different from the case for LHP-1. As shown by Fig. 18, a minimum thermal resistance of LHP-2 achieved at a heat load of 40 W was roughly equal to $R_{\text{cond-sink}}$. Besides, when the heat load was 20 W, the thermal resistance of LHP-2 was at its maximum reaching about 0.78 °C/W, which was much larger than the other two thermal resistances $R_{\text{hs-ev}}$ and $R_{\text{cond-sink}}$. The most possible reason might be attributed to the imperfect contact between the evaporator wall and the wick, leading to a large contact thermal resistance between them and the resultant obvious vapor superheat, which significantly degraded the heat transfer performance of LHP-2. Another possible reason may be the employment of the stainless-steel wick in the evaporator of LHP-2. Because the thermal conductivity of stainless steel (~15 W/m·°C) is much smaller than that of nickel (~90 W/m·°C), it will cause a considerable increase in the thermal resistance from the evaporator wall to the liquid/vapor interface adjacent to the outer surface of the wick for LHP-2, which will also generate obviously superheated vapor there.

As for the thermal resistance of the “heat source-LHP-heat sink” system, because there existed no much difference in the thermal resistances of $R_{\text{hs-ev}}$ and $R_{\text{cond-sink}}$ for LHP-1 and LHP-2, the total thermal resistance of the two heat transfer systems was mainly determined by the thermal resistance of the LHP. According to the experimental results, the minimum value of the total thermal resistance was about 0.55 and 0.78 °C/W for LHP-1 and LHP-2 respectively. It should be of note that according to the standard error transfer equation, the relative uncertainty of the system thermal resistance for LHP-1 and LHP-2 at a heat load greater than 20 W is 10.3% and 7.2%, respectively.

3.3 Effect of gravity

For a two-phase heat transfer device operating in the terrestrial surroundings, the gravity will generally

play an important role in its thermal performance, which should be considered carefully. In this study, the effects of gravity on the thermal performance of the two R134a LHPs were investigated systematically. The relative height of the evaporator ΔH was defined as positive when the evaporator was located higher than the condenser. The LHP operation was in the gravity-assisted mode and antigravity mode in the case $\Delta H < 0$ and $\Delta H > 0$, respectively, based on the relative height between the evaporator and the condenser. In the experiment, the heat sink temperature was always maintained at 20 °C, and the maximum vapor temperature was always controlled below 70 °C for safety consideration.

The heat load dependence of the vapor temperature at different relative heights of the evaporator is shown in Fig. 19. When the condenser was located higher than the evaporator ($\Delta H < 0$), i.e., in the gravity-assisted mode, the steady-state operating temperature curves displayed quite similar trend as that in the anti-gravity mode. However, in this situation, the vapor temperature usually dropped to some extent and the heat transfer limit increased. For instance, in the case that the condenser was elevated 0.1 m higher than the evaporator, the maximum heat load increased by about 30 and 40 W for LHP-1 and LHP-2, respectively.

In the case that the evaporator was elevated above the condenser ($\Delta H > 0$), i.e., in the antigravity mode, the two LHPs manifested quite different thermal responses. According to the experimental results, the operation of LHP-2 seemed to be more sensitive to the adverse elevation, and a few centimeters of adverse elevation would cause a significant decrease of the heat transfer capability. As the elevation of the evaporator was increased from 0 to 0.05 m, the heat transfer limit of LHP-2 decreased from 120 to 40 W. When the evaporator was located 0.10 m higher than the condenser, LHP-2 could not operate stably even at a heat load of 20 W. It could be concluded that the antigravity capability of LHP-2 was rather weak. That is because the pore diameter of the evaporator wick of LHP-2 is relatively large, whose maximum capillary

pressure is about 2.0 kPa at 50 °C based on equation (6). An adverse elevation of 0.05m will produce a gravitational pressure drop of about 0.6 kPa, which will inevitably cause a considerable decrease in the heat transfer capability.

$$\Delta P_{\text{cap, max}} = \frac{2\sigma}{r} \quad (6)$$

On the contrary, even in the case $\Delta H = +0.1$ m, no significant degradation in the heat transfer capacity was observed for LHP-1. This should be attributed to the quite small pore diameter in the evaporator wick, and under which condition a relatively large maximum capillary force (~ 10.0 kPa) can be developed. Certainly, the small pore diameter of the evaporator wick is not always beneficial to the heat transfer capacity, due to the rapid increase of the flow resistance in the wick.

Generally, an ammonia-charged LHP is able to transport a heat load greater than 600 W with strong antigravity capability [35, 36]; while the two LHPs using R134a as the working fluid in this work only have a heat transfer capacity a little larger than 100 W. The obvious decrease in the heat transfer capacity is mainly caused by the difference in the relevant thermo-physical properties. That is because besides the system structural parameters, the heat transfer capacity of a LHP is strongly dependent on the thermo-physical properties of the working fluid especially the liquid surface tension and evaporative latent heat. To be specific, the surface tension determines the maximum capillary pressure that the evaporator wick can produce, which is the main driving force for the circulation of the working fluid in the loop; while the evaporative latent heat represents the energy transported by unit mass of the working fluid, and a large evaporative latent heat corresponds to a small mass flowrate under a fixed heat load applied to the evaporator, which is crucial in affecting the overall pressure drop of the system. As analyzed above, the larger the liquid surface tension and evaporative latent heat, the higher the heat transfer capacity. As shown in Table 3, both the liquid surface tension and evaporative latent heat of R134a are much smaller than those

of ammonia, which should be responsible for the much reduced heat transfer capacity. In addition, the porosity of the wick in this work is not very good, especially for the wick made of stainless steel powders with a porosity of 40.2%. The wick porosity significantly affects its transport characteristics, and generally the smaller the porosity of the wick, the larger the flow resistance in the wick. When R134a is selected as the working fluid, because its evaporative latent heat is small, the mass flowrate in the loop becomes very large accordingly, leading to a large pressure drop in the evaporator wick and the resultant small capillary limit. In order to increase the heat transfer capacity of the LHPs with R134a as the working fluid, the structural parameters of the evaporator wick, both in the macroscopic and microscopic scales, should be appropriately optimized.

4 Conclusions

In this work, two sets of LHPs using environmentally friendly R134a as the working fluid was designed and fabricated, one with a nickel wick and the other with a stainless-steel wick, and an extensive comparative study have been conducted mainly including the startup characteristics, power increment test, thermal resistance analysis and heat transfer capacity. According to the experimental results and theoretical analysis, the main conclusions can be summarized as follows:

- Both of the LHPs using R134a as the working fluid present excellent startup performance, which can realize the startup with slight or no temperature overshoot even in the most difficult startup scenario at very small heat load, ensuring it a totally passive two-phase heat transfer device.
- With stepwise change of the heat load applied to the evaporator, both of the R134a LHPs exhibit good response characteristics, and the operating temperature changes quickly and smoothly, promising great application prospect in modern electronics cooling.
- A minimum LHP thermal resistance of about 0.033 °C/W can be achieved using R134a as the

working fluid, and the minimum value of the total thermal resistance of the “heat source-LHP-heat sink” system is about 0.55 and 0.78 °C/W for LHP-1 and LHP-2 respectively.

- Both of the R134a LHPs can operate at a heat load greater than 100 W with the vapor temperature below 70 °C under the horizontal orientation. In the gravity-assisted mode, the heat transfer capacity can be further enhanced.
- Using a nickel wick with small pore diameter, the R134a LHP shows good anti-gravity capability, and an adverse elevation of 0.1 m will not result in obvious degradation in its heat transfer capability and thermal performance.

This work contributes to a better understanding on the operating performance and characteristics of LHPs using R134a as the working fluid, providing good design guidance and reference for its future practical applications.

Acknowledgement

This work was supported by the National Natural Science Foundation of China (Nos. 51576010 and 51776012) and the Beijing Natural Science Foundation (No. 3182023).

Nomenclature

ΔH	adverse elevation	m
ΔP	pressure difference	Pa
dP	differential of pressure	Pa
dT	differential of temperature	°C
Q	heat load	W
R	thermal resistance	°C/W
r	effective pore radius	m
T	temperature	°C

Greek symbols

σ	surface tension	N/m
----------	-----------------	-----

Subscripts

cap	capillary
cond	condenser
cond-sink	condenser and heat sink
ev	evaporator
hs	heat source
hs-ev	heat source and evaporator
hs-LHP-sink	from heat source to heat sink
LHP	loop heat pipe
max	maximum
sat	saturation
sink	heat sink

References

- [1] G. Xiahou, J. Zhang, R. Ma, et al., Novel heat pipe radiator for vertical CPU cooling and its experimental study, *International Journal of Heat and Mass Transfer* 130 (2019) 912-922.
- [2] A. Faghri, Review and Advances in Heat Pipe Science and Technology, *Journal of Heat Transfer-Transactions of the ASME* 134(12) (2012), paper No. 123001.
- [3] K.S. Kim, M.H. Won, J.W. Kim, et al., Heat pipe cooling technology for desktop PC CPU, *Applied Thermal Engineering* 23(9)(2003) 1137-1144.
- [4] S. Riffat, X. Ma, Recent developments in heat pipe technology and applications: a review, *International Journal of Low Carbon Technologies* 2(2) (2007) 162-177.
- [5] C. Yang, C. Chang, C. Song, et al., Fabrication and performance evaluation of flexible heat pipes for potential thermal control of foldable electronics, *Applied Thermal Engineering* 95 (2016) 445-453.
- [6] X. Chen, H. Ye, X. Fan, et al., A review of small heat pipes for electronics, *Applied Thermal Engineering* 96 (2016) 1-17.
- [7] H. Jouhara, A. Chauhan, T. Nannou, et al., Heat pipe based systems - Advances and applications, *Energy* 128 (2017) 729-754.
- [8] H. Tang, Y. Tang, Z. Wan, et al., Review of applications and developments of ultra-thin micro heat pipes for electronic cooling, *Applied Energy* 223 (2018) 383-400.
- [9] Y.F. Maydanik, Loop heat pipes, *Applied Thermal Engineering* 25 (2005) 635-657.
- [10] S. Launay, V. Sartre, J. Bonjour, Parametric analysis of loop heat pipe operation: a literature review, *International Journal of Thermal Sciences* 46 (2007) 621-636.
- [11] L. Bai, J. Fu, G. Lin, et al., Quiet power-free cooling system enabled by loop heat pipe, *Applied Thermal Engineering* 155 (2019) 14-23.
- [12] T. Hoang, W. Armiger, R. Baldauff, et al., Performance of COMMX Loop Heat Pipe on TacSat 4 Spacecraft, AIAA paper, 2012, No. 3498.
- [13] C. Baker, C. Butler, P. Jester, et al., Geoscience Laser Altimetry System (GLAS) Loop Heat Pipe Anomaly and On Orbit Testing, AIAA paper, 2011, No. 5209.
- [14] R. Yang, G. Lin, J. He, et al., Investigation on the effect of thermoelectric cooler on LHP operation with non-condensable gas, *Applied Thermal Engineering* 110 (2017) 1189-1199.
- [15] J. Rodriguez, A. Na-Nakornpanom, In-Flight Performance of the TES Loop Heat Pipe Heat Rejection System-Seven Years In Space, AIAA paper, 2012, No. 3500.

- [16] Q. Su, S. Chang, Y. Zhao, et al., A review of loop heat pipes for aircraft anti-icing applications, *Applied Thermal Engineering* 130 (2018) 528-540.
- [17] N.S. Ramasamy, P. Kumar, B. Wangaskar, et al., Miniature ammonia loop heat pipe for terrestrial applications: Experiments and modeling, *International Journal of Thermal Sciences* 124 (2018) 263-278.
- [18] V.G. Pastukhov, Y.F. Maidanik, C. V. Vershinin, et al., Miniature loop heat pipes for electronics cooling, *Applied Thermal Engineering* 23 (2003) 1125-1135.
- [19] R. Singh, A. Akbarzadeh, C. Dixon, et al., Miniature loop heat pipe with flat evaporator for cooling computer CPU, *IEEE Transactions on Components and Packaging Technologies* 30(1) (2007) 42-49.
- [20] V.G. Pastukhov, Y.F. Maydanik, Low-noise cooling system for PC on the base of loop heat pipes, *Applied Thermal Engineering* 27 (2007) 894-901.
- [21] W. Zimbeck, G. Slavik, J. Cennamo, et al., Loop heat pipe technology for cooling computer servers, 11th IEEE Intersociety Conference on Thermal and Thermomechanical Phenomena in Electronic Systems, 2008, pp:19-25.
- [22] L. Vasiliev, D. Lossouarn, C. Romestant, et al., Loop heat pipe for cooling of high-power electronic components, *International Journal of Heat and Mass Transfer* 52 (2009) 301-308.
- [23] J.H. Choi, B.H. Sung, J.H. Yoo, et al., Enhanced Miniature Loop Heat Pipe Cooling System for High Power Density Electronics, *Journal of Thermal Science and Engineering Applications*, 4(2) (2012), paper No. 021008.
- [24] T.B. Peters, M. McCarthy, J. Allison, et al., Design of an integrated loop heat pipe air-cooled heat exchanger for high performance electronics, *IEEE Transactions on Components, Packaging and Manufacturing Technology* 2(10)(2012) 1637-1648.
- [25] P. Gunnasegaran, M.Z. Abdullah, N.H. Shuaib, Experimental Analysis and FEM Simulation of Novel Finned Loop Heat Pipe, *Advanced Materials Research* 925(2014) 481-485.
- [26] T. Tharayil, L.G. Asirvatham, S. Rajesh, et al., Thermal Management of Electronic Devices Using Combined Effects of Nanoparticle Coating and Graphene-Water Nanofluid in a Miniature Loop Heat Pipe, *IEEE Transactions on Components, Packaging and Manufacturing Technology* 8 (2018) 1241-1253.
- [27] S. He, J. Zhao, Z. Liu, et al., Experimental investigation of loop heat pipe with a large squared evaporator for cooling electronics, *Applied Thermal Engineering* 144 (2018) 383-391.
- [28] T. Kobayashi, T. Ogushi, S. Haga, et al., Heat transfer performance of a flexible looped heat pipe using R134a as a working fluid: Proposal for a method to predict the maximum heat transfer rate of FLHP, *Heat Transfer-Asian Research* 32(4) (2003) 306-318.
- [29] A.A. Adoni, A. Ambirajan, V.S. Jasvanth, et al., Effects of Mass of Charge on Loop Heat Pipe Operational

- Characteristics, *Journal of Thermophysics and Heat Transfer* 23 (2009) 346-355.
- [30] A.A. Adoni, J.S. Vaidya, A. Ambirajan, et al., Evaporation heat transfer coefficient in a capillary pumped loop and loop heat pipe for different working fluids, *Heat Transfer Engineering* 33(9) (2012) 765-774.
- [31] M. Nishikawara, H. Nagano, Parametric experiments on a miniature loop heat pipe with PTFE wicks, *International Journal of Thermal Sciences* 85 (2014) 29-39.
- [32] J. He, J. Miao, L. Bai, et al., Effect of non-condensable gas on the startup of a loop heat pipe, *Applied Thermal Engineering* 111 (2017) 1507-1516.
- [33] Y. Maydanik, S. Vershinin, M. Chernysheva, et al., Investigation of a compact copper-water loop heat pipe with a flat evaporator, *Applied Thermal Engineering* 31 (2011) 3533-3541.
- [34] L. Bai, G. Lin, D. Wen, et al., Experimental investigation of startup behaviors of a dual compensation chamber loop heat pipe with insufficient fluid inventory, *Applied Thermal Engineering* 29 (2009) 1447-1456.
- [35] Y. Maydanik, V. Pastukhov, M. Chernysheva, Development and investigation of a loop heat pipe with a high heat-transfer capacity, *Applied Thermal Engineering* 130 (2018) 1052-1061.
- [36] V.S. Jasvanth, Abhijit A. Adoni, V. Jaikumar, et al., Design and testing of an ammonia loop heat pipe, *Applied Thermal Engineering* 111 (2017) 1655-1663.

Table captions

Table 1 Basic parameters of the tested LHPs

Table 2 Liquid/vapor distribution in the evaporator

Table 3 Comparison of relevant thermophysical parameters at 20 °C

Figure captions

Fig. 1 Basic structure of a loop heat pipe

Fig. 2 Schematic of the evaporator of LHP-1 and thermocouple locations

Fig. 3 Schematic of the evaporator of LHP-2 and thermocouple locations

Fig. 4 Schematic of the condenser and thermocouple locations

Fig. 5 Startup process of LHP-1 at a heat load of 5W in situation 3

Fig. 6 Startup process of LHP-1 at a heat load of 5W in situation 4

Fig. 7 Startup process of LHP-1 at a heat load of 20W in situation 4

Fig. 8 Startup process of LHP-1 at a heat load of 40W in situation 4

Fig. 9 Startup process of LHP-2 at a heat load of 2W

Fig. 10 Startup process of LHP-2 at a heat load of 20 W

Fig. 11 Startup process of LHP-2 at a heat load of 40W

Fig. 12 Startup process of LHP-2 at a heat load of 80W

Fig. 13 Startup with a large temperature overshoot for ammonia LHP with a heat load of 5W

Fig. 14 Thermal response of LHP-1 in power increment test

Fig. 15 Thermal response of LHP-2 in power increment test

Fig. 16 Steady-state operating characteristics of LHP-1

Fig. 17 Steady-state operating characteristics of LHP-2

Fig. 18 Thermal resistance analysis of the “heat source-LHP-heat sink” system

Fig. 19 Effect of gravity on the thermal performance of the two R134a LHPs

Table 1 Basic parameters of the tested LHPs

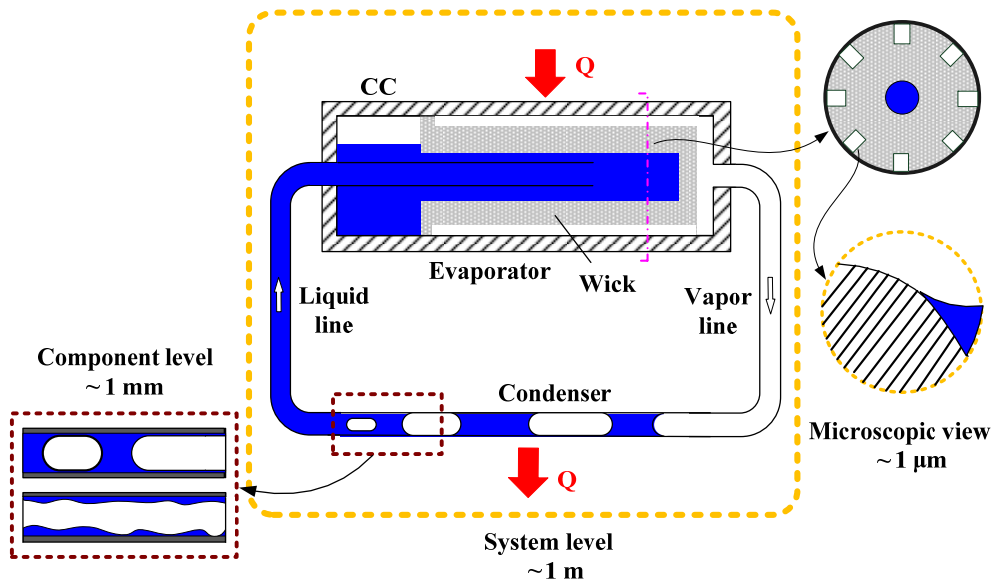
Items		LHP-1	LHP-2
Evaporator casing	Material	Stainless steel	Stainless steel
	OD/ID×length/mm	18/16×130	13/11×90
Wick	Material	Nickel	Stainless steel
	OD/ID×length/mm	16/5×120	11/9×80
	Maximum pore radius/μm	1.0	5.0
	Porosity	55.3%	40.2%
	Permeability	2.6×10^{-14}	8.7×10^{-14}
Vapor grooves	Number×height×width/mm	14×0.5×1.0	10×0.5×1.0
CC	Material	Stainless steel	Stainless steel
	OD/ID×length/mm	30/28×112	36/34×45
	Volume/ml	69.0	41.0
Vapor line	Material	Stainless steel	Stainless steel
	OD/ID×length/mm	6/5×495	6/5×520
Condenser	Material	Stainless steel	Stainless steel
	OD/ID×length/mm	6/5×640	6/5×640
Liquid line	Material	Stainless steel	Stainless steel
	OD/ID×length/mm	6/5×785	6/5×720
Charged amount		112g	71g

Table 2 Liquid/vapor distribution in the evaporator

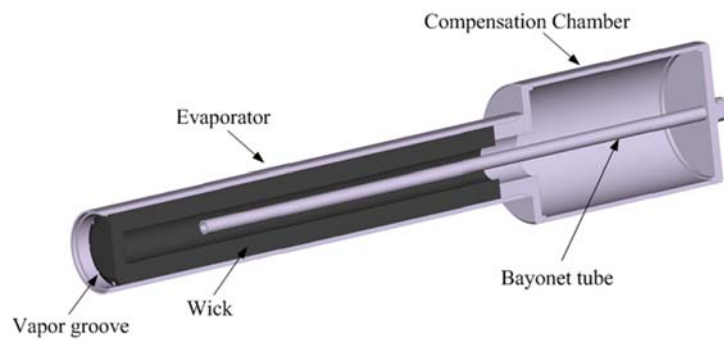
Startup situation	Vapor grooves/evaporator core
1	Liquid filled/liquid filled
2	Vapor exists/ liquid filled
3	Liquid filled /vapor exists
4	Vapor exists/vapor exists

Table 3 Comparison of relevant thermophysical parameters at 20 °C

Working fluid	$dP/dT _{\text{sat}}$ [kPa/°C]	Evaporative latent heat [kJ/kg]	Surface tension[mN/m]
Ammonia	27.4	1160.0	26.4
R134a	17.7	182.4	8.4



(a) System structure



(b) Internal structure of the evaporator and compensation chamber

Fig. 1 Basic structure of a loop heat pipe

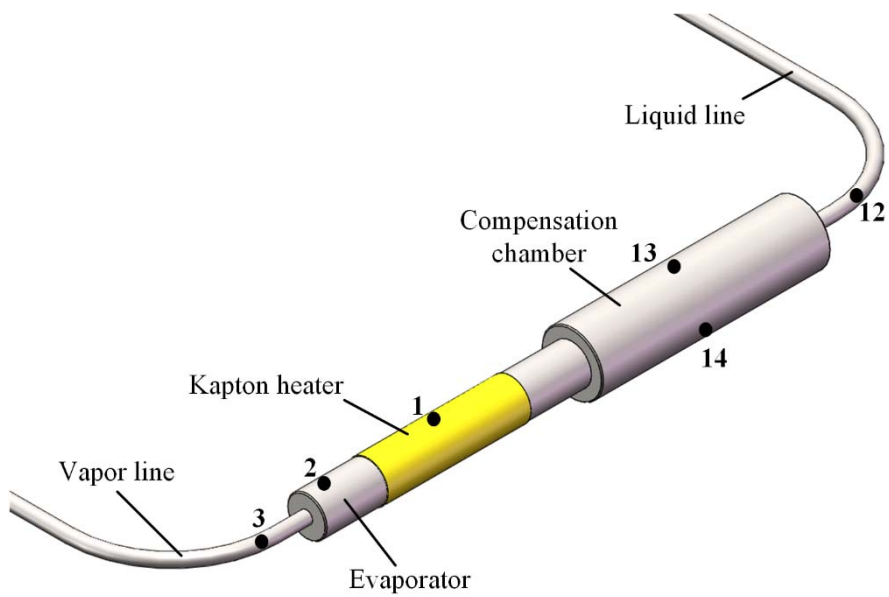


Fig. 2 Schematic of the evaporator of LHP-1 and thermocouple locations

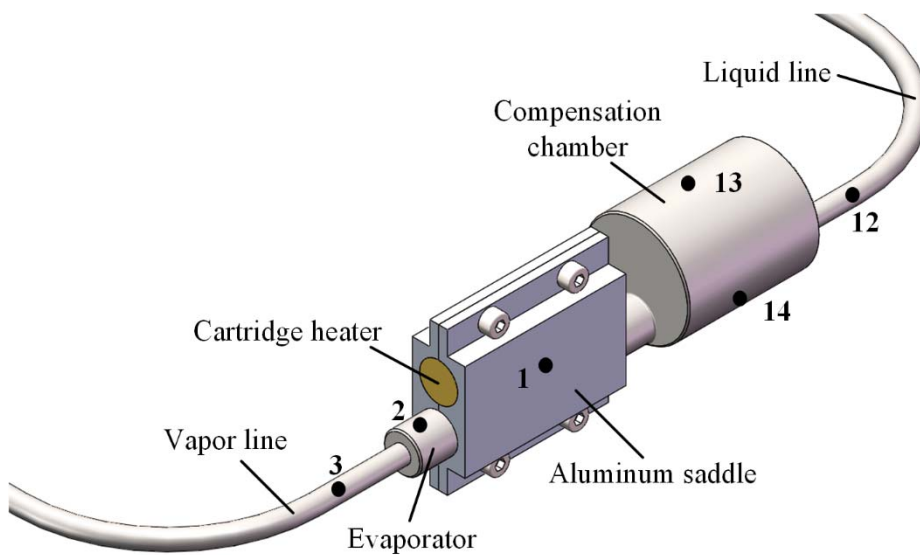


Fig. 3 Schematic of the evaporator of LHP-2 and thermocouple locations

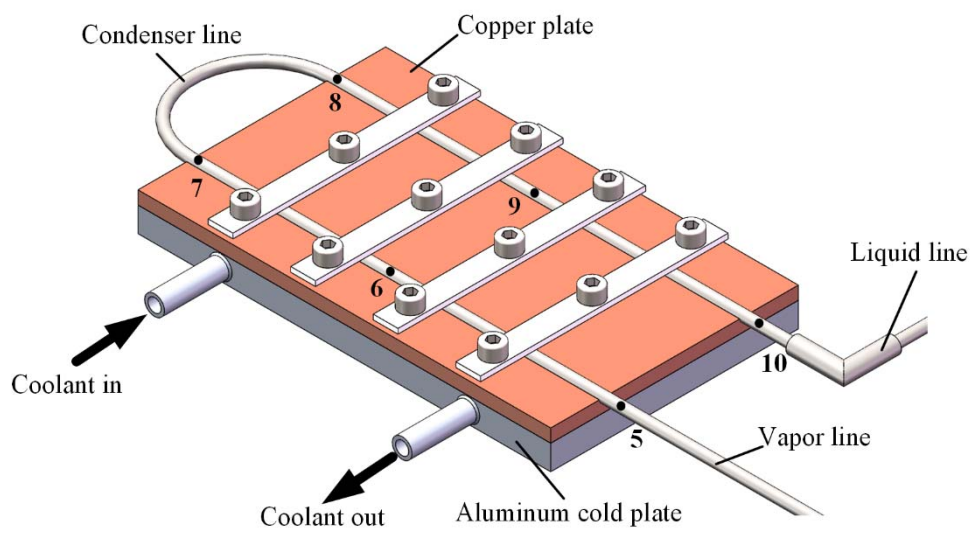


Fig. 4 Schematic of the condenser and thermocouple locations

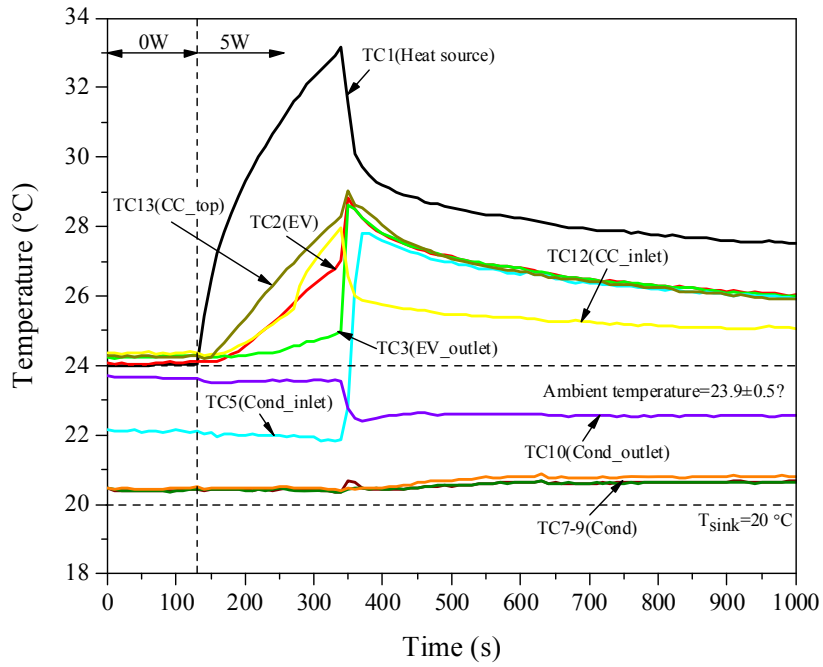


Fig. 5 Startup process of LHP-1 at a heat load of 5W in situation 3

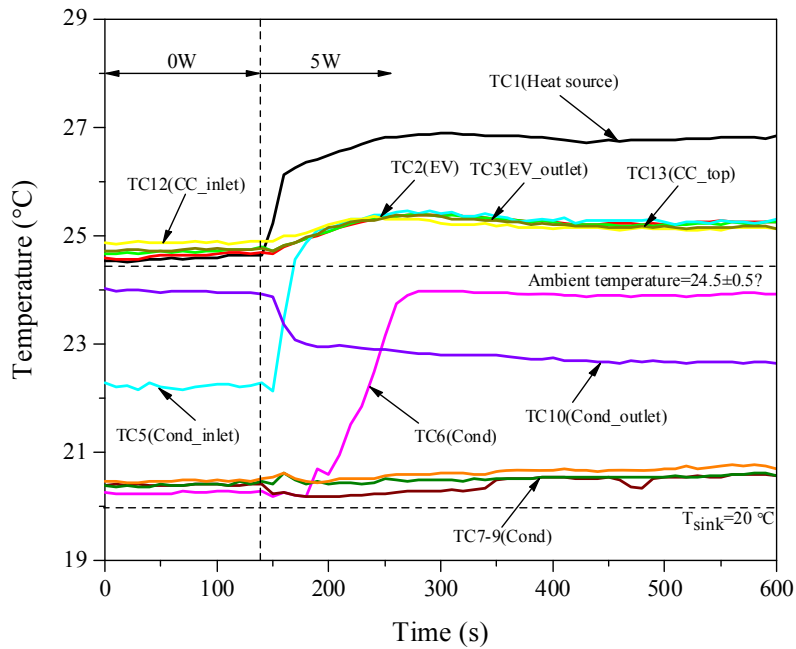


Fig. 6 Startup process of LHP-1 at a heat load of 5W in situation 4

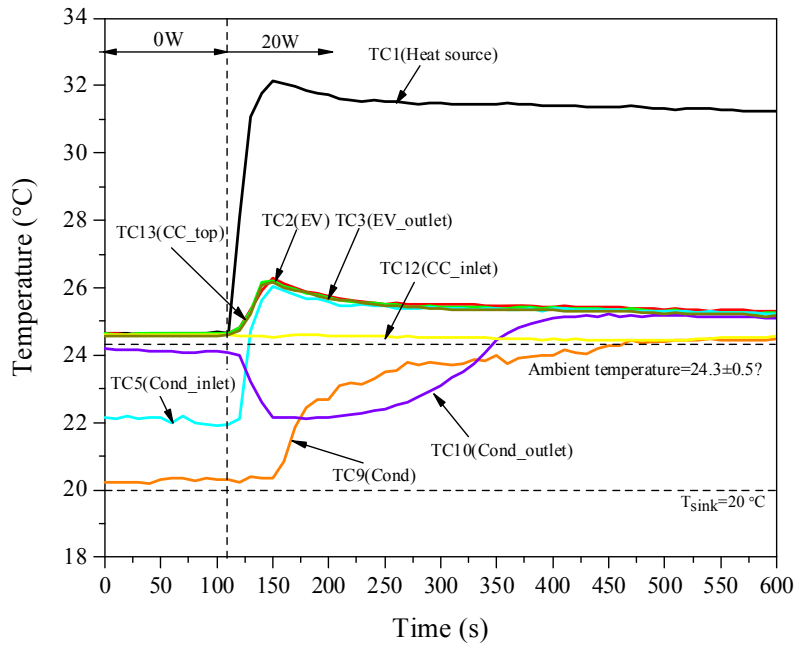


Fig. 7 Startup process of LHP-1 at a heat load of 20W in situation 4

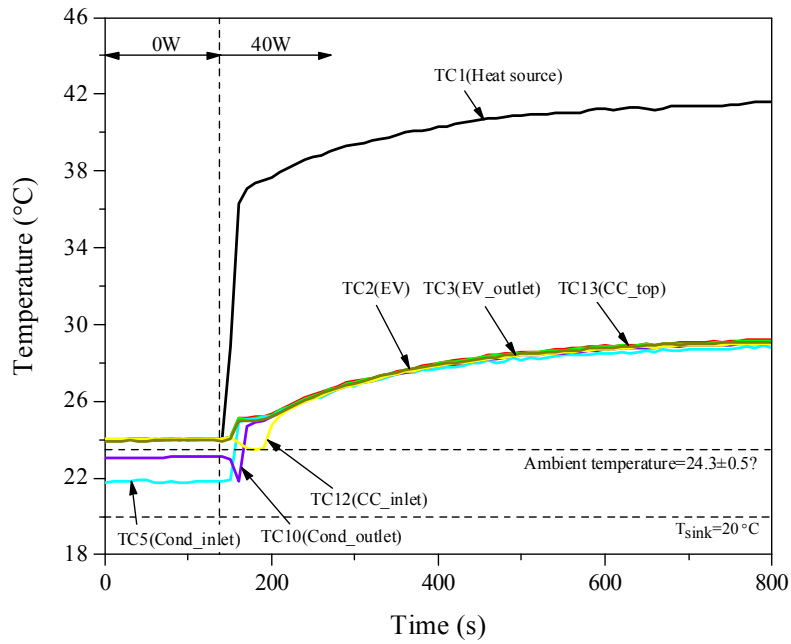


Fig. 8 Startup process of LHP-1 at a heat load of 40W in situation 4

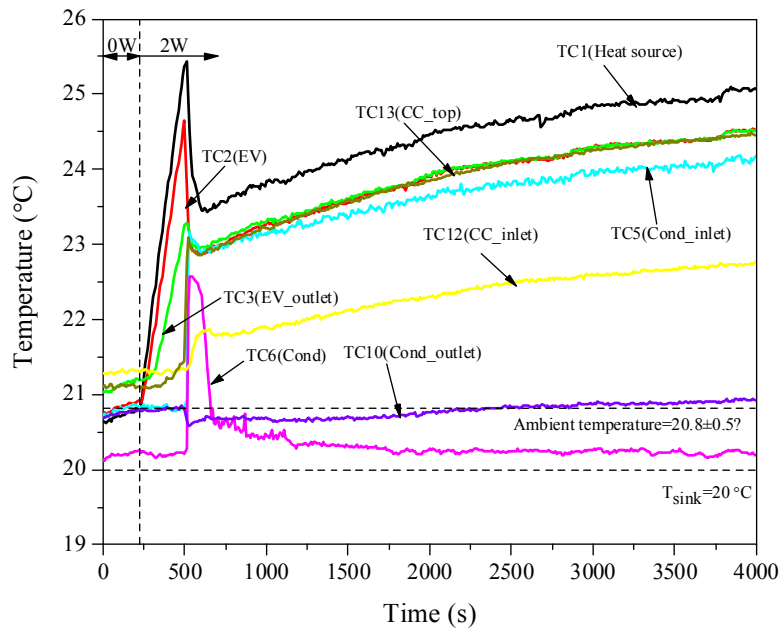


Fig. 9 Startup process of LHP-2 at a heat load of 2W

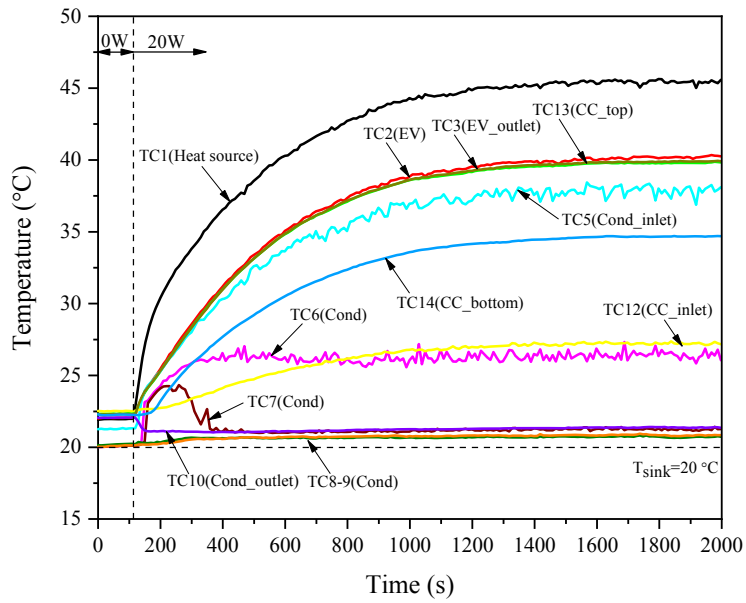


Fig. 10 Startup process of LHP-2 at a heat load of 20 W

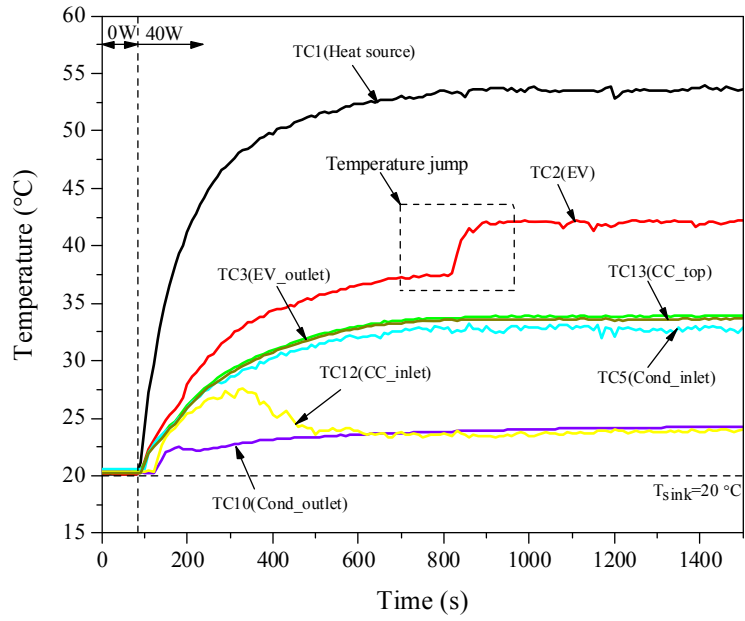


Fig. 11 Startup process of LHP-2 at a heat load of 40W

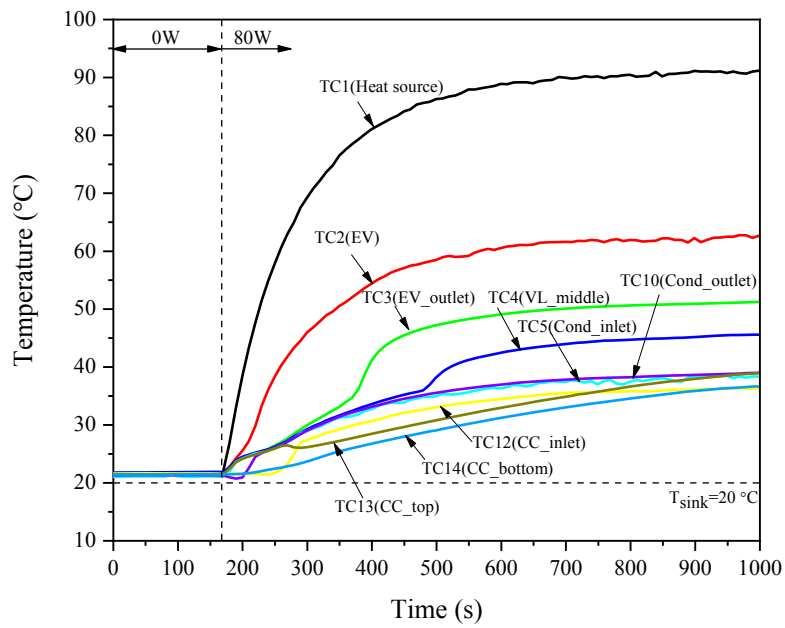


Fig. 12 Startup process of LHP-2 at a heat load of 80W

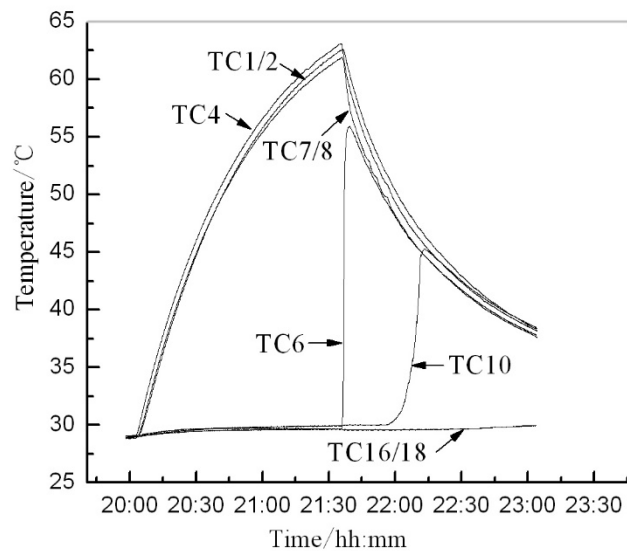


Fig. 13 Startup with a large temperature overshoot for ammonia LHP with a heat load of 5W

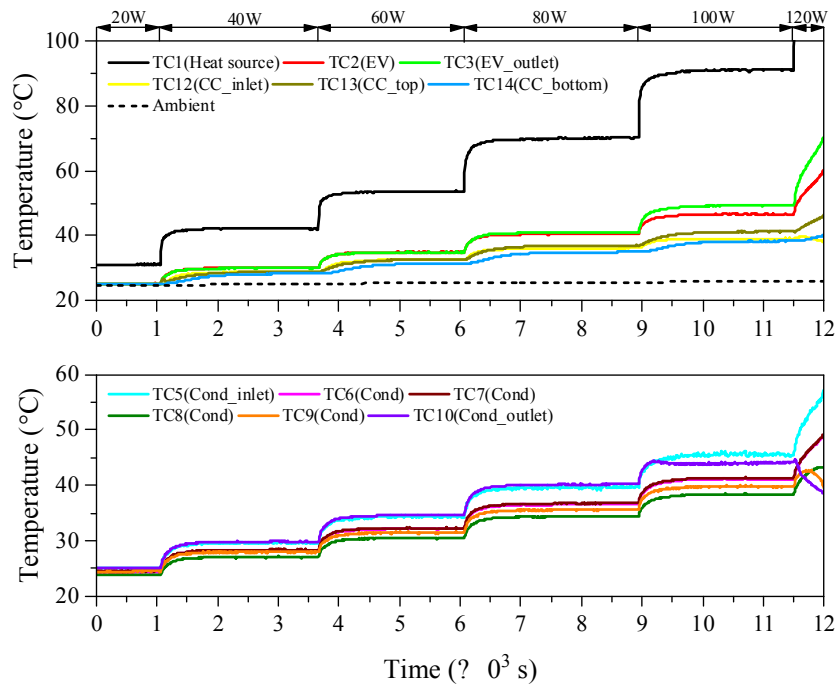


Fig. 14 Thermal response of LHP-1 in power increment test

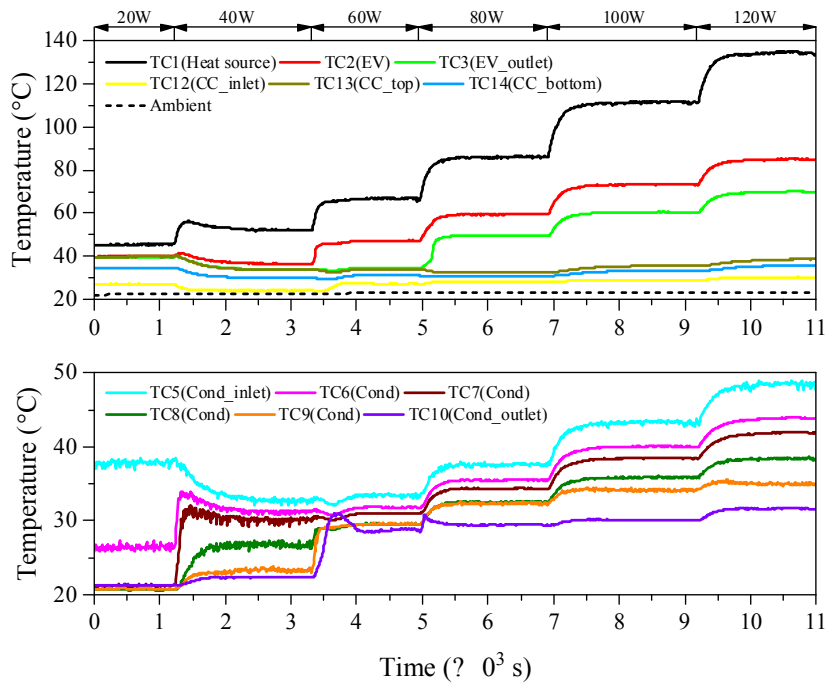


Fig. 15 Thermal response of LHP-2 in power increment test

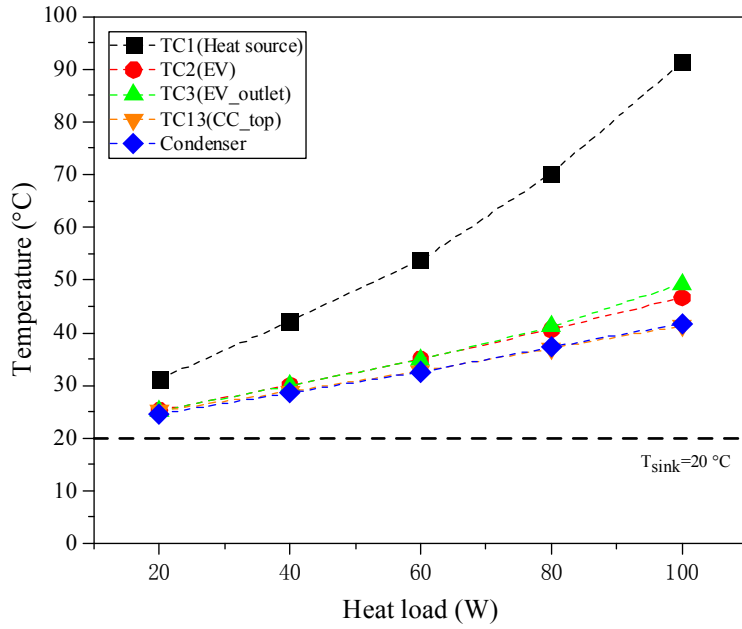


Fig. 16 Steady-state operating characteristics of LHP-1

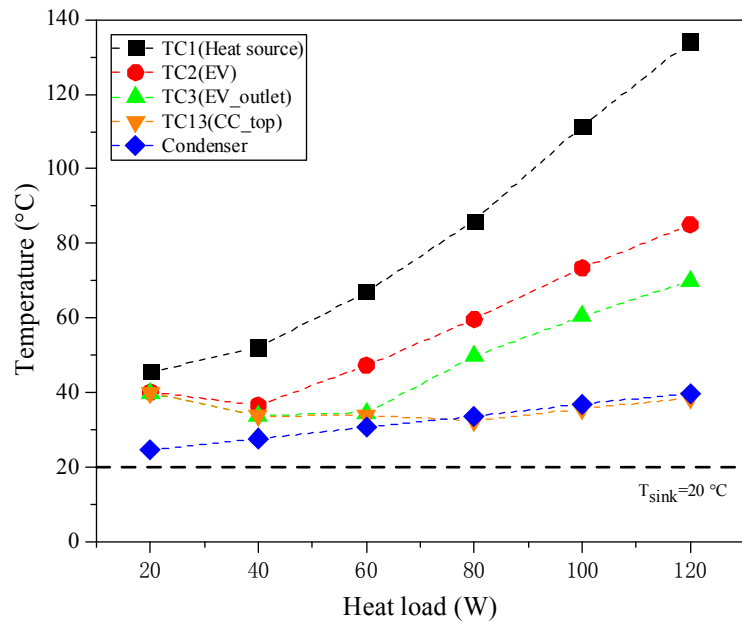
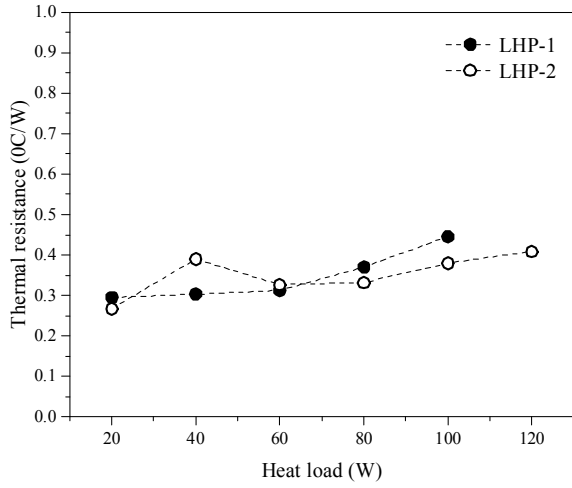
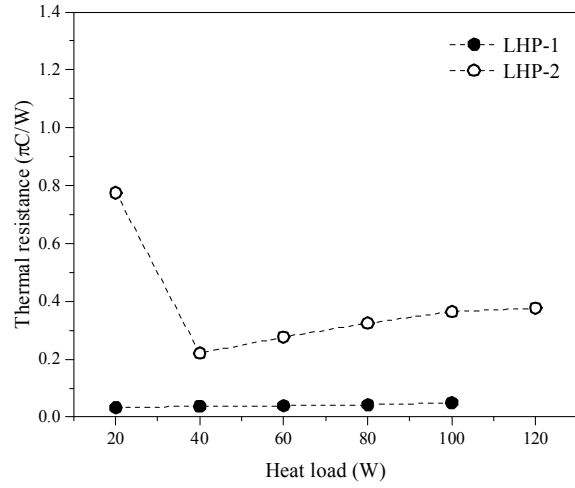


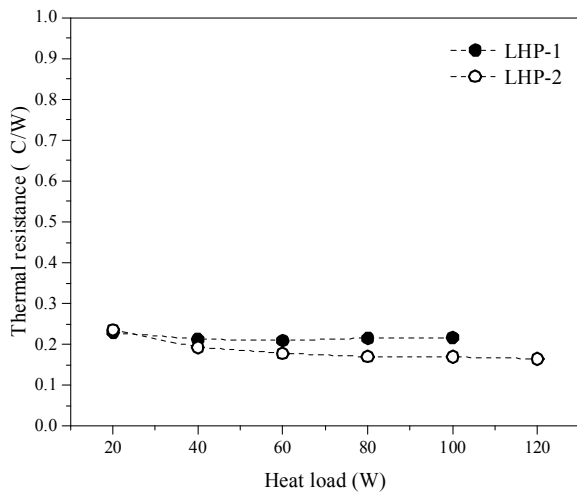
Fig. 17 Steady-state operating characteristics of LHP-2



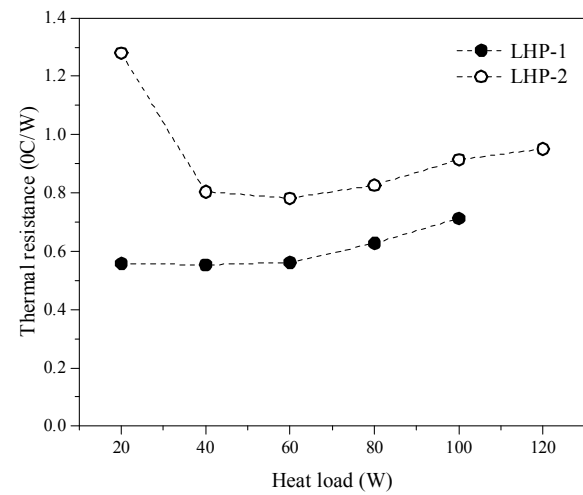
(a) Thermal resistance from heat source to the evaporator



(b) Thermal resistance of the loop heat pipe



(c) Thermal resistance from the condenser to heat sink



(d) System thermal resistance from heat source to heat sink

Fig. 18 Thermal resistance analysis of the “heat source-LHP-heat sink” system

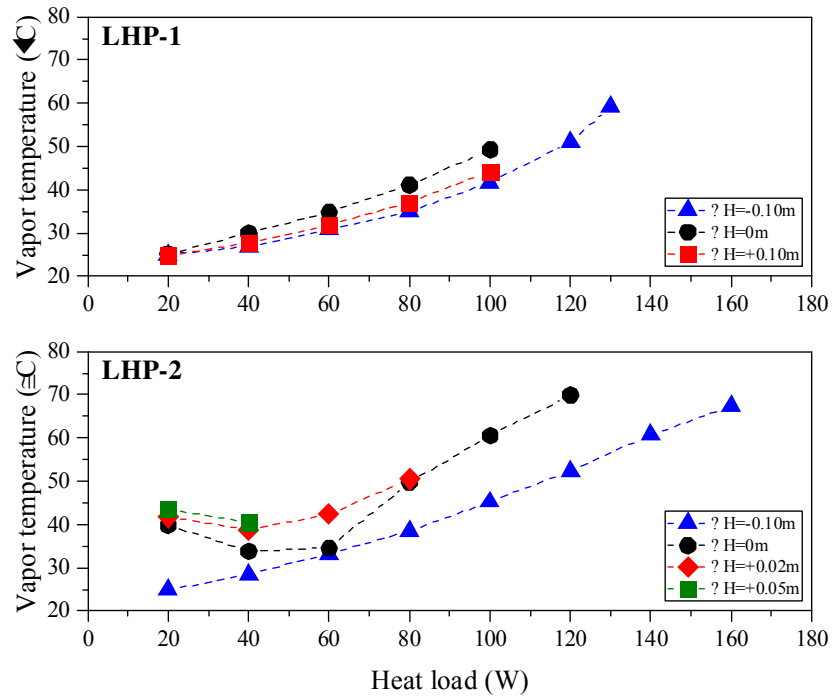


Fig. 19 Effect of gravity on the thermal performance of the two R134a LHPs